nature astronomy
LETTERS
https://doi.org/10.1038/s41550-021-01308-0

Optical and ultraviolet pulsed emission from an accreting millisecond pulsar

F. Ambrosino[1,2,3,22] ✉, A. Miraval Zanon[4,5,22] ✉, A. Papitto[1], F. Coti Zelati[5,6,7], S. Campana[5], P. D'Avanzo[5], L. Stella[1], T. Di Salvo[8], L. Burderi[9], P. Casella[1], A. Sanna[9], D. de Martino[10], M. Cadelano[11,12], A. Ghedina[13], F. Leone[14], F. Meddi[3], P. Cretaro[15], M. C. Baglio[5,16], E. Poretti[5,13], R. P. Mignani[17,18], D. F. Torres[6,7,19], G. L. Israel[1], M. Cecconi[13], D. M. Russell[16], M. D. Gonzalez Gomez[13], A. L. Riverol Rodriguez[13], H. Perez Ventura[13], M. Hernandez Diaz[13], J. J. San Juan[13], D. M. Bramich[16] and F. Lewis[20,21]

Millisecond spinning, low-magnetic-field neutron stars are believed to attain their fast rotation in a 0.1–1-Gyr-long phase during which they accrete matter endowed with angular momentum from a low-mass companion star[1]. Despite extensive searches, coherent periodicities originating from accreting neutron star magnetospheres have been detected only at X-ray energies[2] and in ~10% of the currently known systems[3]. Here we report the detection of optical and ultraviolet coherent pulsations at the X-ray period of the transient low-mass X-ray binary system SAX J1808.4−3658, during an accretion outburst that occurred in August 2019[4]. At the time of the observations, the pulsar was surrounded by an accretion disk, displayed X-ray pulsations and its luminosity was consistent with magnetically funnelled accretion onto the neutron star. Current accretion models fail to account for the luminosity of both optical and ultraviolet pulsations; these are instead more likely to be driven by synchro-curvature radiation[5,6] in the pulsar magnetosphere or just outside of it. This interpretation would imply that particle acceleration can take place even when mass accretion is going on, and opens up new perspectives in the study of coherent optical/ultraviolet pulsations from fast-spinning accreting neutron stars in low-mass X-ray binary systems.

Low-mass X-ray binary (LMXB) systems hosting a weakly magnetic ($\sim 10^{8}$ G) neutron star are believed to be progenitors of millisecond radio pulsars. The evolutionary link between the two classes was first demonstrated through the detection of fast coherent X-ray pulsations generated by accretion onto the neutron star magnetic poles and the ensuing lighthouse effect in several transient LMXB systems[2,7]. Definitive proof came with the discovery of a small group of transitional millisecond binary pulsars that alternate between rotation-powered and accretion-powered states[8,9]. Fast coherent pulsations and their frequency evolution in accreting neutron star systems are a tool of fundamental importance to determine binary parameters and accretion torques, investigate the properties of disk–magnetosphere interaction and magnetically funnelled accretion, and derive constraints on the equation of state of ultradense matter[10]. Through the detection and precise determination of the spin and orbital ephemeris of LMXB systems, especially the most luminous and closest ones, it is also possible to carry out tuned, increased sensitivity searches for gravitational waves at (twice) the neutron star rotational frequency. Fast accretion-powered coherent pulsations have proven elusive: in more than three decades they were detected at X-ray energies in 22 (refs. [3,11,12]) out of ~190 LMXB systems harbouring neutron stars[13], all of which are transient systems attaining peak luminosities of up to several per cent the Eddington limit. So far, optical pulsations have been detected only from the transitional millisecond pulsar PSR J1023+0038 (ref. [14]), during an X-ray sub-luminous disk state[15]. Both the X-ray and optical pulsations of this system, which happen almost exactly at unison, are believed to originate from synchrotron radiation in the intrabinary shock just beyond the light cylinder radius, where the wind of relativistic particles ejected by the pulsar meets the accretion disk[15–17].

The transient LMXB system SAX J1808.4−3658 is the first-discovered accreting millisecond X-ray pulsar[2]. The pulsar spins with a period of 2.49 ms and orbits an ~0.04 $M_{\odot}$ companion star[18] with a 2 h orbital period[7]; it is located at a distance[19] of about 3.5 kpc. Since its discovery in 1996, the source underwent nine ~1-month-long outbursts during which the X-ray source luminosity[20] reached typically a few 10^{36} erg s^{-1}, starting from a quiescence level[21] of $\sim 5 \times 10^{31}$ erg s^{-1}. The higher mass inflow rate giving rise to the X-ray outbursts also causes an increase in the source ultraviolet (UV) and optical brightness by ~4 and ~3.5 magnitudes,

---

[1] INAF-Osservatorio Astronomico di Roma, Rome, Italy. [2] INAF-Istituto di Astrofisica e Planetologia Spaziali, Rome, Italy. [3] Sapienza Università di Roma, Rome, Italy. [4] Dipartimento di Scienza e Alta Tecnologia, Università dell'Insubria, Como, Italy. [5] INAF-Osservatorio Astronomico di Brera, Lecco, Italy. [6] Institute of Space Sciences (ICE, CSIC), Barcelona, Spain. [7] Institut d'Estudis Espacials de Catalunya (IEEC), Barcelona, Spain. [8] Dipartimento di Fisica e Chimica, Università degli Studi di Palermo, Palermo, Italy. [9] Dipartimento di Fisica, Università degli Studi di Cagliari, Monserrato, Italy. [10] INAF-Osservatorio Astronomico di Capodimonte, Naples, Italy. [11] Dipartimento di Fisica e Astronomia, Università di Bologna, Bologna, Italy. [12] INAF-Osservatorio di Astrofisica e Scienze dello Spazio di Bologna, Bologna, Italy. [13] Fundación Galileo Galilei - INAF, Tenerife, Spain. [14] Sezione Astrofisica, Dipartimento di Fisica e Astronomia, Università di Catania, Catania, Italy. [15] INFN-Sezione di Roma 1, Rome, Italy. [16] Center for Astro, Particle, and Planetary Physics, New York University Abu Dhabi, Abu Dhabi, United Arab Emirates. [17] INAF-Istituto di Astrofisica Spaziale e Fisica Cosmica Milano, Milan, Italy. [18] Janusz Gil Institute of Astronomy, University of Zielona Góra, Zielona Góra, Poland. [19] Institució Catalana de Recerca i Estudis Avançats (ICREA), Barcelona, Spain. [20] Faulkes Telescope Project, School of Physics and Astronomy, Cardiff University, Cardiff, Wales, UK. [21] Astrophysics Research Institute, Liverpool John Moores University, Liverpool, UK. [22] These authors contributed equally: F. Ambrosino, A. Miraval Zanon. ✉e-mail: filippo.ambrosino@inaf.it; arianna.miraval@inaf.it

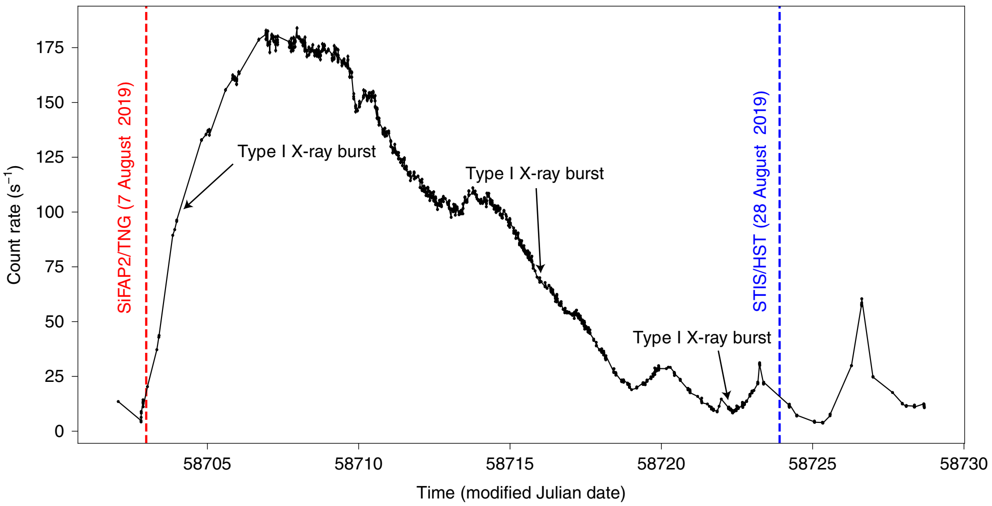

Fig. 1 | XTI/NICER X-ray light curve (0.5–10 keV) of the August 2019 outburst of SAX J1808.4−3658. The red and the blue dashed lines indicate the epoch of our optical (7 August 2019) and UV (28 August 2019) fast-photometry observations. Intervals including type I X-ray bursts have been removed from the plot. The epoch of their occurrence is indicated by arrows.

as a result of enhanced irradiation of the companion star and outer disk regions[22] by the X-rays from the inner disk region and the neutron star[20,23].

In the summer of 2019, SAX J1808.4−3658 underwent another outburst[4], attaining a peak 0.5–10 keV luminosity of ~10^{36} erg s^{-1} on 12 August, after an ~5 day rise. A decay followed and, starting from 24 August, ~4–5-day-long luminosity oscillations took place between ~10^{34} erg s^{-1} and ~10^{35} erg s^{-1}. Repeated observations with the X-ray Timing Instrument (XTI) on board the Neutron Star Interior Composition Explorer (NICER) closely monitored the evolution of the outburst and X-ray pulsations (Fig. 1), yielding refined measurements of the neutron star spin period and orbital parameters (see Methods and ref. [4]). On 7 August, during the rising phase of the outburst when the X-ray luminosity was ~6×10^{34} erg s^{-1}, we observed the source for ~1 h with the Silicon Fast Astronomical Photometer (SiFAP2)[14], operating in the 320–900 nm band and mounted at the Telescopio Nazionale Galileo (TNG) in La Palma. An ~2 ks observation was carried out on 28 August with the Space Telescope Imaging Spectrograph (STIS), operating in the 165−310 nm UV band, on board the Hubble Space Telescope (HST), when the X-ray luminosity was ~3.4×10^{34} erg s^{-1} in the final oscillating stages of the outburst (Fig. 1).

The Fourier power density spectra of the high-timing-resolution optical and UV light curves are shown in Fig. 2. In both cases, a narrow peak is present at the ~401 Hz spin frequency of the neutron star, with a probability of random occurrence in a single frequency bin of 5.1×10^{-8} and 2.3×10^{-6} in the optical and UV data, respectively. The optical and UV pulsed light curves folded at the X-ray spin period reported in Table 1 and displaying a single-peaked quasi-sinusoidal profile are shown as insets in Fig. 2. The background-subtracted root mean square (r.m.s.) amplitude of the optical pulsations was (0.55 ± 0.06)%, corresponding to $L_{\mathrm{pulsed(opt)}}\approx2.7\times10^{31}$ erg s^{-1} (the total 325–690 nm optical luminosity was $L_{\mathrm{opt}}\approx5\times10^{33}$ erg s^{-1}). In the XTI/NICER observations that covered the epoch of the SiFAP2/TNG observation, the X-ray pulsations had an ~9 times larger r.m.s. amplitude (4.8 ± 0.3%), and a factor ~100 higher luminosity, $L_{\mathrm{pulsed(X)}}\approx2.3\times10^{33}$ erg s^{-1}, than the optical pulsations (see Methods for details). Interestingly, the optical pulsation profile was shifted in phase by $\Delta\phi=0.55\pm0.02$ (or $\Delta\tau=1.38\pm0.06$ ms in time) with respect to that in the X-rays, that is, virtually in anti-phase. We note that PSR J1023+0038 does not show such a feature as its optical and X-ray pulse profiles are almost in phase (time lag of ~200 μs)[15].

The UV coherent pulsations detected during the STIS/HST observation were (relatively) stronger than the optical pulsations from 3 weeks earlier: their (2.6 ± 0.7)% r.m.s. amplitude led to a pulsed 165–310 nm luminosity of $L_{\mathrm{pulsed(UV)}}=0.026L_{\mathrm{UV}}\approx2\times10^{32}$ erg s^{-1}. Correspondingly, the X-ray pulsations detected during the NICER observation carried out a few hours later had a (5.7 ± 0.9)% r.m.s. amplitude, and involved a factor of ~10 higher pulsed X-ray luminosity of $L_{\mathrm{pulsed(X)}}\approx1.9\times10^{33}$ erg s^{-1}. Owing to the large uncertainties on the absolute timing of the HST data (~1 s, HST helpdesk private communication), the relative phasing of the UV and X-ray profiles could not be determined.

The presence of type I X-ray bursting activity as well as X-ray luminosities exceeding the spin-down power measured in quiescence[4] (1.6×10^{34} erg s^{-1}) by up to two orders of magnitude testify that the outbursts of SAX J1808.4−3658 are powered by mass accretion. Also at the time of the SiFAP2/TNG and STIS/HST observations, the X-ray luminosity was higher than the spin-down power by a factor of ~2 and 4 (though the pulsed X-ray luminosity was lower). Moreover the source X-ray spectral and timing properties evolved moderately and continuously across the luminosity swing of the outburst (as well as that of previous outbursts) down to ~10^{34} erg s^{-1} without displaying any evidence for transitions to a non-accreting regime[4]. The X-ray pulsations were likely generated by funnelled accretion onto the magnetic pole. Here we report the SAX J1808.4−3658 optical/UV pulsations, detected nearly simultaneously with the X-ray pulsations, during the accretion phase of a millisecond spinning neutron star. In the following we discuss their possible origin.

Thermal emission from warm concentric rings surrounding the polar caps can be ruled out because, even considering a large emitting area (~100 km^2), the temperature should attain unrealistically high values (>1 MeV) to generate the observed optical and UV fluxes. For the coherent signals not to be smeared out by light travel time delays, projection of their emission region along the line of sight should be smaller than $cP_{\mathrm{spin}}/2\approx300-400$ km, where c is the speed of light in vacuum and P_{spin} is the pulsar spin period. If the UV/optical pulsations arose from optically thick emission or reprocessing, the ~2.7×10^{31} erg s^{-1} optical pulsed luminosity would imply a temperature of ~$2(l\ /\ 300\,\mathrm{km})^{-2}$ keV, where l is the size of the emitting region, and a bolometric luminosity of ~$10^{41}(l\ /\ 300\,\mathrm{km})^{-6}$ erg s^{-1}, making this model untenable. Moreover, the maximum size of this region limits the amount of energy that can be re-emitted for reprocessing of X-ray pulsations in the outer region of the disk

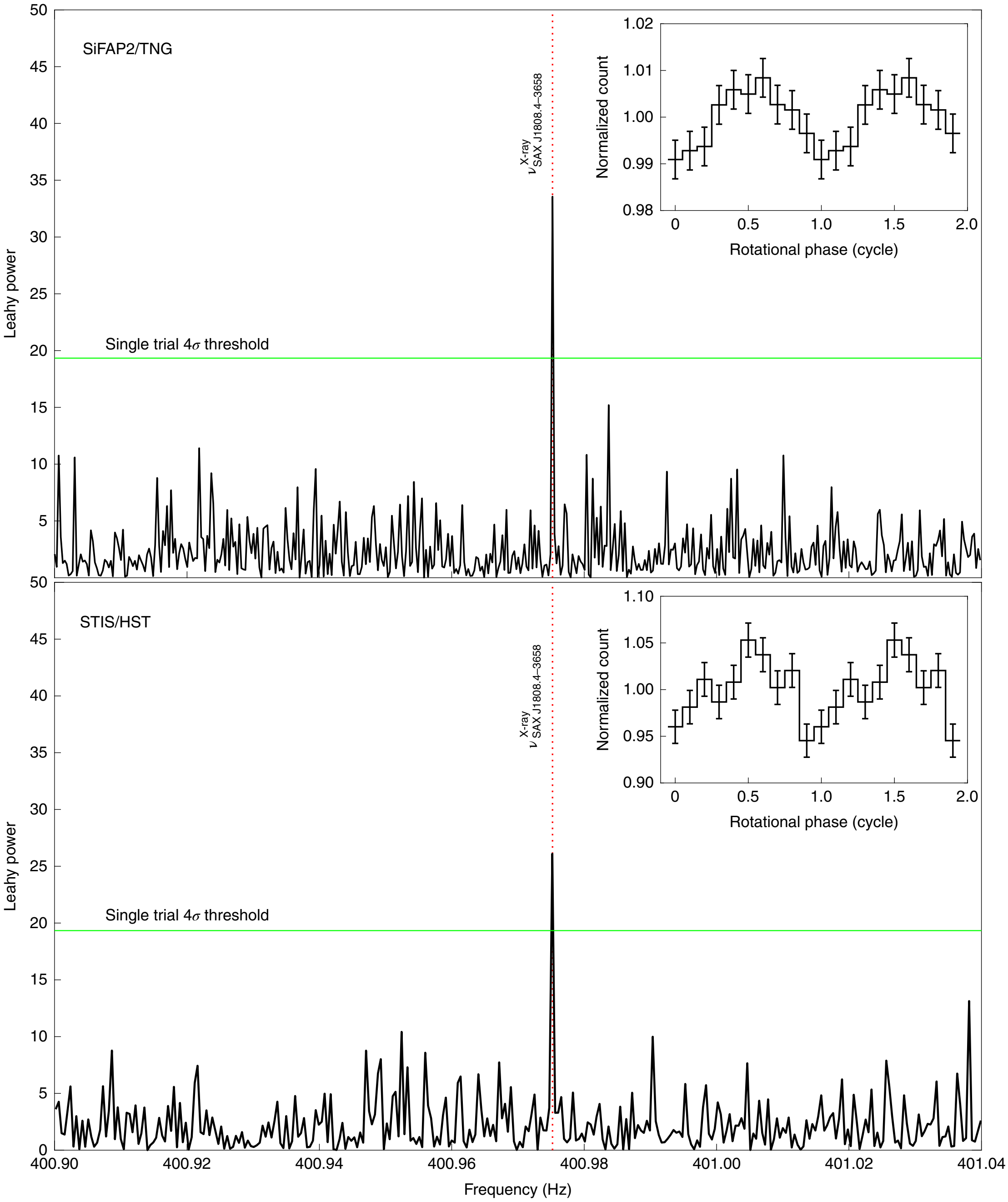

Fig. 2 | Detection and shape of coherent optical and UV signals from SAX J1808.4−3658. Upper panel: Fourier power density spectrum of the optical (320–900 nm) light curve from the 3.3 ks observation carried out with the SiFAP2 photometer mounted at the TNG, starting on 7 August 2019 at 22:31 (coordinated universal time, UTC). Only a zoomed region around the expected spin frequency of SAX J1808.4−3658 is shown. Once corrected for the systematic drift of the SiFAP2 system clock (see Methods), photon arrival times were converted to the Solar System barycentre and then corrected for the pulsar orbital motion using the X-ray ephemeris reported in Table 1. The light curve was binned at 100 μs, corresponding to a Nyquist frequency of 5 kHz. Lower panel: Fourier power density spectrum over the same frequency range from the UV (165–310 nm) light curve collected with STIS on board HST during a 2.2 ks observation starting on 28 August 2019 at 21:47 UTC. UV photon arrival times were first processed with the ODELAYTIME task (see Methods) to shift them to the Solar System barycentre, and then corrected for the pulsar orbital motion using the same X-ray ephemeris reported in Table 1. The light curve was rebinned to 500 μs, yielding a Nyquist frequency of 1 kHz. The dotted red vertical line marks the spin frequency of SAX J1808.4−3658 from the X-ray ephemeris, whose uncertainty on the spin frequency is small enough that only a single trial frequency has to be examined. The highest peaks in both panels coincide with this frequency, to within their Fourier resolution (see Methods). The green horizontal lines mark the power level corresponding to a probability of 6.3×10^{-5} (4σ) of being exceeded by white noise in a single frequency bin. The insets show the background-subtracted, normalized pulse profiles obtained by folding the optical and UV light curves at the X-ray period (Table 1); two cycles are plotted for clarity. Phases refer to the reference epoch of the SiFAP2 and STIS observations, respectively; errors bars are 1σ.

($R_{\text{out}} \approx (2\text{–}3)\times10^{10}$ cm) to $\sim10^{29}$ erg s^{-1} in the 320–900 nm band, even in the most favourable case of an inclination of 90°. The problem with this interpretation would be exacerbated if reprocessing or energy release in optically thick matter occurred in regions of size comparable to the characteristic scales of SAX J1808.4−3658, namely the neutron star radius ($R_{\text{NS}} \approx 10$ km), the inner disk boundary close

Table 1 | X-ray, UV and optical ephemeris of SAX J1808.4−3658 during the August 2019 outburst

Parameter	X-ray	UV	Optical
Right ascension[a] (α, J2000)	18 h 08 m 27.62 s	–	–
Declination[a] (δ, J2000)	−36° 58′ 43.3″	–	–
Validity range (MJD)	58702–58726		
Reference epoch $T_{\rm ref}$ (MJD)	58715.0	–	–
Time system	TDB	TDB	TDB
Planetary ephemeris	DE405	DE200	DE405
Spin frequency ($\nu(T_{\rm ref})$) (Hz)	400.975209660(9)	–	–
Spin frequency ($\nu(T_{\rm TNG})$)[b] (Hz)	400.975210179(63)	–	400.975225(72)[d]
Spin frequency ($\nu(T_{\rm HST})$)[c] (Hz)	400.975209618(36)	400.97517(10)[d]	–
Spin frequency first derivative ($\dot{\nu}$) (Hz s^{-1})	$-(2.43\pm0.21)\times10^{-13}$	–	–
Spin frequency second derivative ($\ddot{\nu}$) (Hz s^{-2})	$(4.9\pm1.1)\times10^{-19}$	–	–
Orbital period ($P_{\rm b}$) (s)	7249.1572(14)	–	–
Time of ascending node ($T^{\star}$) (MJD)	58715.0220987(32)	–	–
Projected semi-major axis (light seconds)	0.0628099(35)	–	–
χ^2/d.o.f.	550/378	–	–

[a]Values taken from ref. [39]. [b]Observation carried out on 7 August 2019 ($T_{\rm Start}^{\rm TNG}$ = 58702.9382176 MJD(UTC)) with SiFAP2/TNG. [c]Observation carried out on 28 August 2019 ($T_{\rm Start}^{\rm HST}$ = 58723.9080081 MJD(UTC)) with STIS/HST. [d]Obtained with the epoch folding search technique. d.o.f., degrees of freedom; MJD, modified Julian date; TDB, barycentric dynamical time.

to the corotation radius ($r_{\rm c} = (GM_{\rm NS}P^2_{\rm spin}/4\pi^2)^{1/3} \approx 32$ km, where G is the gravitational constant and $M_{\rm NS}$ is the neutron star mass) or the light cylinder radius ($r_{\rm lc} = cP_{\rm spin}/2\pi \approx 120$ km); in fact, all these regions are smaller than ~300 km.

Hot electrons in the post-shock region of the accretion column will emit cyclotron photons at a fundamental energy of $E_{\rm cyc} \approx 4(r/R_{\rm NS})^{-3}$ eV, where r is the parametric radial distance, for a surface magnetic field of SAX J1808.4−3658 of $B \approx 3.5\times10^8$ G (ref. [24]). If the optically thick regime extended up to the nth cyclotron harmonic, a Rayleigh–Jeans spectrum would result up to the corresponding energy[25]. For SAX J1808.4−3658 the maximum expected luminosity would be $L_{\rm cyc(opt)} \approx 10^{29}$ erg s^{-1} in the 320–900 nm band, and $L_{\rm cyc(UV)} \approx 6\times10^{29}$ erg s^{-1} in the 165–310 nm band (see Methods), that is, more than two orders of magnitude lower than the measured values. Therefore, it can also be excluded that self-absorbed cyclotron emission in the accretion column is responsible for the optical/UV pulsed flux of SAX J1808.4−3658, unless emission in these bands is strongly beamed, which is deemed unlikely given the high pulse duty cycle. Also, pencil beaming due to the reduction of the cyclotron opacity for photons propagating along the field lines[26] is expected at energies much lower than $E_{\rm cyc}$, that is, below the optical band within which we observed. These limitations would no longer hold if the optical/UV pulsed emission were produced by a coherent emission process[27], whose specific intensity can vastly exceed that of thermal emission. However, we note that coherent emission from rotation-powered pulsars is characterized by a steep power-law-like radio spectrum and is not expected to operate at much higher frequencies.

Similar to the case of isolated rotation-powered pulsars[28], synchro-curvature radiation[5,6] by relativistic electrons and positrons accelerated by the rotating neutron star magnetosphere might give rise to the optical and UV pulsations of SAX J1808.4−3658. In this interpretation, the efficiency with which SAX J1808.4−3658 converts the spin-down power into pulsed UV and optical luminosity would be $\eta_{\rm UV} \approx 1\times10^{-2}$ and $\eta_{\rm opt} \approx 6\times10^{-4}$, respectively, the former being about 100 times larger than that of the Crab pulsar in the UV (165–310 nm) and B bands[29] (see Methods). Such a high efficiency is much larger than that usually observed for isolated rotation-powered pulsars, and points towards the existence of a synergistic physical process.

Models based on magnetohydrodynamic simulations[30] predict that the neutron star magnetic field lines coupled to the disk within the corotation radius are rapidly twisted, pushed outwards and forced to open[31], a phenomenon possible only in accreting millisecond X-ray pulsars with high magnetic diffusivity disks. In this picture, the rotation-powered mechanism would not be inhibited by the presence of the accretion disk; rather its power would increase (as compared with diskless pulsars) owing to the opening of additional magnetic field lines and the corresponding flux enhancement across the light cylinder surface. This leads to an increase of the spin-down torque applied to the neutron star and a stronger electromagnetic pulsar wind[30]. A net spin-down rate of the order of $\sim -1\times10^{-13}$ Hz s^{-1} would be expected in the case of SAX J1808.4−3658. We note that a comparably large spin-down torque and rate may arise from magnetic field lines threading the disk beyond the corotation radius[32]. If the high optical and UV pulsed luminosities of SAX J1808.4−3658 result from an enhanced rotation-powered mechanism, this must coexist (or alternate on a timescale shorter than those required to detect pulsations with current instrumentation) with the accretion-powered mechanism that produces the X-ray pulsations. Alternatively, the power of the so-called striped wind[33] may also be enhanced by the same disk–magnetosphere interaction. In this model, part of the pulsar spin-down power is carried away in the form of low-frequency waves consisting of stripes of toroidal magnetic field; these structures propagate along the equatorial plane of the pulsar and are converted into a wind of relativistic magnetized plasma beyond the light cylinder radius through magnetic reconnection. In this framework, the optical and UV pulsations from SAX J1808.4−3658 would arise from beamed synchrotron radiation by heated charged particles moving close to the light cylinder radius[34]. Here, synchrotron radiation is optically thin to emission in the UV and optical bands, as synchrotron self-absorption occurs below[35] $E_{\rm break} \approx 0.04$ eV. Optical/UV pulsed emission from synchrotron radiation is still expected at distances $\lesssim 600$ km from the neutron star, considering that the synchrotron cooling timescale is shorter than $P_{\rm spin}/2$. The efficiency of this process could be enhanced at the termination shock between the pulsar wind and the accretion disk[15–17].

An intriguing feature is the half-cycle shift between the optical and the X-ray pulsations from SAX J1808.4−3658. It is tempting to consider the possibility that matter accretion takes place only on one pole of the neutron star, thus giving rise to the pulsed X-ray signal, whereas accretion is inhibited on the opposite side and a rotation-powered mechanism gives rise to the optical/UV pulsation in anti-phase. A dipole magnetic field whose centre is shifted from the centre of the neutron star might make this possible.

The discovery of optical and UV pulsations during the accretion outburst of a millisecond X-ray pulsar shows that particle acceleration mechanisms can occur even in regimes where the magnetosphere is engulfed with accreting plasma for at least a substantial fraction of the time. Moreover, it opens a novel observational window in the study of accreting neutron stars in LMXB systems, as the higher sensitivity afforded by optical and UV fast photometric observations may allow the discovery of coherent pulsations in sources and regimes for which X-ray pulsations have remained undetected.

Methods

TNG optical observation. The optical dataset of SAX J1808.4−3658 was collected with SiFAP2[36] (TNG Director Discretionary Time, principal investigator A. Papitto) mounted at the Nasmyth A focus of the INAF 3.58 m Telescopio Nazionale Galileo (TNG), located on the Roque de los Muchachos Observatory in La Palma (Canary Islands, Spain). SiFAP2, the upgraded version of SiFAP[37,38], is a two-channel ultra-fast photometer operating in the optical band (320–900 nm) capable of tagging the time of arrival of individual photons with a time resolution of 8 ns. The absolute timing is provided by a commercial global positioning system (GPS) unit via the pulse-per-second signal with a nominal 25 ns accuracy on the coordinated universal time (UTC) worsened to less than 60 μs because of the SiFAP2 electronics transfer function. This value was obtained from observations performed on the Crab pulsar for calibration purposes[15]. We carried out a single 3.3 ks observation of SAX J1808.4−3658 starting on 7 August 2019 at 22:31 (UTC), during the earliest stage of the outburst. The optical light curve of the source collected with SiFAP2 is shown in Supplementary Fig. 1. No filter was used during our run. The telescope elevation above the horizon was ~24° corresponding to an airmass of ~2.5, while seeing conditions varied within the range from 0.5 up to 0.9 arcsec (at the zenith). The Moon was at an angular distance of 47° from the target, increasing the background contribution by ~70%. During the acquisition, we also measured the sky background signal (taking into account also a dark count rate of $1.8\times10^3\ \mathrm{s}^{-1}$ for the sensors) by moving the telescope 10 arcsec away from the target towards the east direction twice during the observation, for about 30 s each time. We obtained an average count rate of $\mathrm{BKG}_{\mathrm{TNG}} = (34{,}953\pm86)\ \mathrm{s}^{-1}$, representing a contribution of more than 90% of the total count rate, $R_{\mathrm{TNG}} = (38{,}560.6\pm6.5)\ \mathrm{s}^{-1}$, collected by pointing the telescope in the direction of SAX J1808.4−3658. A reference star, TYC 7403−655 − 1 (right ascension (RA) = 18:07:56.38, declination (dec) = −36:55:07.35, V = 12.19 mag) located 432 arcsec away from SAX J1808.4−3658 was also simultaneously observed to monitor the atmospheric variations as well as to verify the absence of spurious periodic signals due to instrumental noise at the pulsar spin frequency. As occurred also in previous observing runs, the SiFAP2 clock drifted by $\Delta t = 5.2$ ms with respect to the time measured by two GPS pulse-per-second signals used to mark the beginning and the end of the observation. We corrected the arrival times assuming that the drift evolved following a linear function of time. This procedure already proved to be efficient in recovering the pulse frequency of both the Crab pulsar and the millisecond pulsar PSR J1023+0038[14,15]. Laboratory tests showed that the thermal jitter of the SiFAP2 system clock could be safely neglected because its relative uncertainty for millisecond spin periods is several tens of times smaller than our measurements[14]. The photon arrival times obtained in this way were then referred to the Solar System barycentre (TDB time system) using the position of the optical counterpart provided by ref. [39] and the geocentric location of the TNG (X = 5,327,447.4810 m, Y = −1,719,594.9272 m, Z = 3,051,174.6663 m), along with the JPL DE405 ephemeris.

UV observation. We observed SAX J1808.4−3658 with the STIS (GO/DD-15987, principal investigator M. Zanon) on board the HST starting on 28 August 2019 at 21:47 (UTC) during the latest stage of the outburst. The UV light curve of the source acquired with STIS is shown in Supplementary Fig. 1. The spectroscopic observation was performed in TIME-TAG mode with 125 μs time resolution for about 2.2 ks by means of the near ultraviolet multi-anode micro-channel array (NUV-MAMA) detector. We used the G230L grating equipped with a 52 × 0.2 arcsec slit ensuring a spectral resolution of ~500 over the nominal range (first order). The total count rate collected by the instrument was $R_{\mathrm{HST}} = (2{,}016.74\pm0.95)\ \mathrm{s}^{-1}$, with a background contribution of about 30%, $\mathrm{BKG}_{\mathrm{HST}} = (653.36\pm0.54)\ \mathrm{s}^{-1}$. The background signal was estimated by selecting photons in the STIS slit channels outside the source region (see 'Timing analysis' section) and averaging them. The resulting value was then normalized to the total number of slit channels.

X-ray observations. The XTI[40] on board NICER[41] observed the SAX J1808.4−3658 outburst[4] from 30 July until 16 September 2019 for a total exposure time of 387.7 ks. The events across the 0.2–12 keV band were processed and screened using HEASOFT version 6.28 and NICERDAS version 7a. We applied standard cleaning and filtering criteria, selecting only the time intervals during which the pointing offset from the nominal source position was smaller than 0.015°, the source was at least 30° away from the Earth limb (at least 40° in the case of a Sun-illuminated Earth) and the International Space Station was outside the South Atlantic Anomaly. The photon arrival times were corrected for the motion in the Solar System barycentre (TDB time system) using the position of the optical counterpart[39] and the JPL DE405 ephemeris. The X-ray light curve of the source outburst from 7 August to 31 August 2019 is shown in Fig. 1. We removed type I X-ray bursts that occurred in the time intervals 58704.81059–58704.81186 MJD, 58716.08876–58716.09104 MJD and 58722.41759–58722.41921 MJD.

Timing analysis. We measured the X-ray pulsar spin and orbital parameters by analysing the observations performed by NICER between 7 and 31 August (that is, MJD 58702–58726). We corrected the arrival times using the orbital parameters previously measured[4]. We folded 1-ks-long segments of NICER data in 16 phase bins around a preliminary estimate of the pulse period[4]. We fitted the pulse profiles with a single sinusoidal component, modelled the evolution of the pulse phases with a function composed of a third-order polynomial and terms resulting from corrections to the orbital parameters (see, for example, ref. [42]), and obtained the timing solution listed in Table 1. This solution is characterized by a χ^2 of 550 for 378 degrees of freedom, indicating a formally unacceptable fit. However, even adopting higher-order polynomials, the fit quality did not improve significantly. No trend is apparent in the residuals shown in the bottom panel of Supplementary Fig. 2, and we attribute the high fit reduced χ^2 to the phase timing noise that is known to affect the phases observed from this and other accreting millisecond X-ray pulsars[12]. The X-ray timing solution derived here is only aimed at performing a search for optical/UV pulses, and modelling such a timing noise component is beyond the scope of this paper. However, we note that Bult et al.[4] derived a timing solution measuring the pulse phases in each continuous good time interval (generally longer than 1 ks) and considering either a second-order polynomial or a flux-adjusted phase model in an attempt to model the timing noise, and obtained similar values of the fit χ^2 than that reported here. The different models used by those authors explain the slight differences between their ephemeris and the ones we obtained. In any case, we checked that our results do not change when using their ephemeris.

Since the TNG observation lasted 3.3 ks, the spacing of Fourier independent frequencies was $\delta\nu_{\mathrm{TNG}} = 3.0\times10^{-4}$ Hz. This is ~5,000 times coarser than the uncertainties on the X-ray spin frequency evaluated at the epoch of the TNG observation ($\sigma_\nu(T_{\mathrm{TNG}}) = 6.3\times10^{-8}$ Hz, see Table 1). After both the barycentric correction and the demodulation for the pulsar orbital motion had been applied, only a single trial frequency had to be searched in the TNG dataset to investigate the presence of a coherent signal at the same frequency as determined from the analysis of the X-ray data. We calculated the Fourier power density spectrum of the TNG light curve and measured a Leahy normalized[43] power of 33.6 at a frequency of 400.97522(15) Hz. The single-trial probability associated with random white noise fluctuations is $p = 5.1\times10^{-8}$. We note that no significant peak at the expected pulsar spin frequency was found in either the power density spectrum of the light curve in which orbital demodulation was not applied or in the reference star light curve. A precise knowledge of the spin and orbital ephemeris were thus essential for detecting the optical (and UV) coherent modulation at the spin period. To refine the measurement of the frequency of the optical pulse, we performed an epoch folding search[44] adopting 10 phase bins and a period stepsize of $\delta P_{\mathrm{TNG,EFS}} = 9.4\times10^{-11}$ s measuring a χ^2 value of $S_{\max} = 38.6$ with a corresponding best-fitting period of $P_{\mathrm{TNG,EFS}} = 0.00249391967(45)$ s. The 1σ uncertainty reported in parentheses was computed[44] by using the equation $\sigma_P = P^2/(2T_{\exp})(S_{\max}/(n-1)-1)^{-0.63}$, where $T_{\exp}$ is the total exposure time of the TNG optical observation. In addition, we also performed the bin-free Z_n^2 test[45] assuming a purely sinuosidal profile shape ($n = 1$), obtaining a value of $Z_1^2 = 34.3$ associated with a best-fitting folding period of $P_{\mathrm{TNG},Z_1^2} = 0.00249391976(62)$ s. This value is compatible with that estimated from the X-ray data within the uncertainties. We report the computed χ^2 distribution with the best-fitting Gaussian model in Supplementary Fig. 3. We then folded the TNG optical light curve using the X-ray pulse parameters, and modelled the pulse profile obtained in this way (inset of Fig. 2) using a single sinusoidal component with a r.m.s. amplitude of (0.051 ± 0.005)%. Taking into account the background (see above), we then estimated the source r.m.s. amplitude as $A_{\mathrm{TNG}}^{\mathrm{r.m.s.}} = (0.55\pm0.06)\%$. Folding at the same spin frequency the SiFAP2/TNG light curve and the XTI/NICER light curve extracted over the time interval between 7 August at 19:18:49 and 8 August at 00:34:55 UTC (a subset of observation ids. 2050260109 and 2050260110) highlighted a phase difference of $\Delta\phi = (0.55\pm0.02)$, corresponding to a time lag of $\tau = (1.38\pm0.06)$ ms (Supplementary Fig. 4)[15], estimated a SiFAP2 absolute timing accuracy of <60 μs, whereas the corresponding NICER values is <0.3 μs, both much lower than the uncertainty affecting the lag measured. To estimate the effect of any residual relative timing uncertainty caused by, for example, the uncertainty on the time dependence of the SiFAP2 clock drift, we assumed that the frequency of the optical and X-ray signals were exactly equal, and estimated the phase uncertainty driven by a frequency drift of an amount equal to the measurement error ($\sigma_\nu = 5\times10^{-5}$ Hz; see Table 1), obtaining a maximum lag of 0.4 ms. Future observations ensuring a full-orbit coverage will confirm the significance and magnitude of the pulse lag.

Hints for slight variations of the optical pulse amplitude were found, although their significance is low. The observed (that is, not subtracted for the background) r.m.s. amplitude varied between (0.07 ± 0.01)% and (0.04 ± 0.01)% over 0.8-ks-long intervals. The TNG optical observation covered about one half the orbital period, from phase 0.04 to 0.49, that is, from shortly after ascending node (phase 0) to close to descending node (phase 0.5). The coherent signal was detected at all phases, although the maximum r.m.s. amplitude was detected when the pulsar was close to the ascending node. Given the intrinsic weakness of the signal, the TNG optical observation was too short to allow us to derive the orbital parameters of the optical pulse from a pulse timing analysis of that dataset. To confirm the association of the optical coherent signal with the pulsar in SAX J1808.4−3658, we then determined the variation of the signal strength by varying the orbital parameters adopted in the correction of the photon arrival times with respect to the values measured from the analysis of the X-ray pulsations. We re-ran the epoch folding periodicity search of the light curves by allowing the epoch of the ascending node ($T^\star$), and the projected semi-major axis ($x = a \sin i / c$) to vary over a grid of values spaced by $\delta T^\star = 2.5$ s and $\delta x = 1\times10^{-3}$ light seconds. The folding period was allowed to vary. The distributions of χ^2 values associated with the best folding period computed by varying independently $T^\star$ and x are reported in Supplementary Fig. 5 and in Supplementary Fig. 6, respectively. We performed a Gaussian fitting on both the χ^2 distributions obtaining the position of the two centroids at $\Delta T^\star = -(4.4\pm2.3)$ s, and $\Delta(a \sin(i) / c) = -(0.32\pm0.33)$ light milliseconds. However, we caution that a coverage of an entire orbital cycle seems warranted to draw firm conclusions on the significance of a possible offset between the two pulse profiles.

We then analysed the UV events obtained from the observation performed with STIS. We corrected the position of slit channels thanks to an external custom function (https://github.com/Alymantara/stis_photons) and selected events (that is, time of arrivals) belonging to channels of the slit within the 991−1,005 (edges excluded) interval to isolate the source signal and minimize the background contribution. We also selected the 165–310 nm wavelength interval to avoid noisy contribution due to the poor response of the G230L grating at the edge wavelengths. The list of good time of arrivals was corrected to the Solar System barycentre by using the ODELAYTIME task (subroutine available in the IRAF/STDAS software package) and the JPL DE200 ephemeris. We applied the same procedure as previously done for SiFAP2 data on the STIS dataset to search for the UV pulsed emission from SAX J1808.4−3658. After demodulating the UV photons' time of arrivals by correcting them for the Rømer delays due to the orbital motion, we computed the Fourier power density spectrum. We found a Leahy normalized[43] power of 26.1 at a frequency of 400.97518(22) Hz, indicating coherent UV pulsations around the expected pulsar spin frequency with an associated single-trial probability of 2.3×10^{-6}. As in the case of the optical dataset, no significant peak at the expected pulsar spin frequency was found in the power density spectrum of the non-demodulated light curve. We then performed an epoch folding search using $n = 10$ phase bins and a period resolution of $\delta P_{\mathrm{HST,EFS}} = 1.4\times10^{-10}$ s. We measured a χ^2 value of $S_{\mathrm{max}} = 39.6$, and a best-fitting period of $P_{\mathrm{HST,EFS}} = 0.00249391998(64)$ s, well in agreement, within the uncertainties, with the period from the X-ray data. The 1σ uncertainty reported in parentheses was computed as in the optical dataset. We report the computed χ^2 distribution with the best-fitting Gaussian model in Supplementary Fig. 3. We performed the bin-free Z_n^2 test with a $n = 1$ component, deriving a value of $Z_1^2 = 29.0$ associated with a best-fitting folding period of $P_{\mathrm{HST},Z_1^2} = 0.00249391997(98)$ s. We then folded the HST UV data at the best period obtained from the X-ray timing analysis (Table 1), and plotted the background-subtracted pulse profile in the inset of Fig. 2. We described the shape of the UV modulation with a single Fourier component with r.m.s. fractional amplitude $A_{\mathrm{HST}}^{\mathrm{r.m.s.}} = (2.6\pm0.7)\%$; note, however, that the rise to the peaks of the modulation was slower than the decay.

Spectral energy distribution. Supplementary Fig. 7 shows the spectral energy distribution (SED) of the total and pulsed emissions in the optical, UV and X-ray bands during the 7 August 2019 observations. The optical and UV magnitudes were corrected for interstellar extinction using the empirical relation[46] $A_V = N_{\mathrm{H}}/(2.87\pm0.12)\times10^{21}$ cm^{-2}, where $N_{\mathrm{H}} = 2.1\times10^{21}$ cm^{-2} is the hydrogen column density along the line of sight to SAX J1808.4−3658 (ref. [47]). We used the extinction curves in ref. [48] to obtain the reddening A_λ in different bandpasses[49]. The optical monitoring data in the B, V, R, i′ bands (B, V, R in the Vega system and i′ in the AB system) were taken with the 2 m Faulkes Telescope South (at Siding Spring, Australia) and Las Cumbres Observatory (LCO) 1 m robotic telescopes in Chile, South Africa and Australia (see refs. [50,51]). The Faulkes/LCO magnitudes were calculated using the X-ray Binary New Early Warning System (XB-NEWS; see refs. [52,53] for details) data analysis pipeline. To estimate the optical flux of SAX J1808.4−3658 at the epoch of our SiFAP2 observation, we interpolated the data of the LCO/Faulkes light curve. The SAX J1808.4−3658 outburst was also monitored with the Ultraviolet and Optical Telescope (UVOT)[54] on board the Neil Gehrels Swift Observatory[55] using different UV filters. The UV counterpart was detected in ten consecutive observations carried out between 6 August and 14 September. The dereddened magnitude measured in the UVOT. UVM2 filter on 7 August (central wavelength of 224.6 nm and full-width at half-maximum of 49.8 nm) was 14.4 ± 0.1 mag (Vega system). For the X-ray band, we extracted the background-subtracted spectrum from the same event file used above to evaluate the phase difference between the X-ray and optical pulses, employing the nibackgen3C50 background modelling tool available at https://heasarc.gsfc.nasa.gov/docs/nicer/tools/nicer_bkg_est_tools.html (total exposure time of ~2.7 ks). We assigned the latest versions of the NICER redistribution matrix ('nixtiref20170601v002.rmf') and ancillary response file ('nixtiaveonaxis20170601v004.arf') to the spectrum, and grouped it so as to contain at least 200 counts in each energy channel. The spectral analysis was performed with the Xspec package[56] (version 12.11.1) and was limited to the energy band between 0.5 and 5 keV, where the source was above the background.

The SED, from optical and UV wavelengths to X-rays, is well fitted by a continuum model consisting of the sum of a blackbody, modelled by bbodyrad in Xspec, and a comptonization component, modelled with nthcomp[57]. To account for the effects of photoelectric absorption by neutral matter in the interstellar medium, we included in the spectral fit the Tuebingen–Boulder model, adopting the photoionization cross-sections from ref. [58] and the chemical abundances from ref. [59]. The equivalent hydrogen column density was held fixed at $N_{\mathrm{H}} = 2.1\times10^{21}$ cm^{-2} in the spectral fit[47,60]. Results are listed in Supplementary Table 1. In this case, the best-fitting value of the blackbody temperature is $kT_{\mathrm{BB}} = 332\pm4$ eV, with an estimated radius of the (spherical) emission region of 3.58 ± 0.08 km for a distance to the source of 3.5 kpc. For the nthcomp component, we fixed the electron temperature and photon index to the best-fitting values found for the broadband X-ray spectrum (kT_{e} fixed at 50 keV and the photon index fixed at 1.9 (ref. [61]), corresponding to an optical depth of about 2 for the comptonization region). We obtained a seed-photon temperature of $kT_{\mathrm{seed}} = 1.48\pm0.03$ eV, in the hypothesis of a blackbody spectrum for the seed photons. We can therefore evaluate the radius of the emitting (spherical) region of the seed photon spectrum by using the relation given by ref. [62]. We find a radius ~10^{1}−10^{11} cm, which is compatible with the inferred size of the accretion disk in this system. This may indicate that the source of seed photons for the comptonization may come from the outer regions of the system, which may contribute to most of the optical/UV emission of the source. This is in agreement with the widely accepted paradigm that most of the optical/UV emission in (black hole or neutron star) LMXB systems is produced in the outer regions of the accretion disk as the result of X-ray reprocessing[63–65].

To obtain a more physical interpretation of the broadband emission of SAX J1808.4−3659, we fitted the SED using a model that accounts for the emission of a truncated accretion disk irradiated by a hot comptonizing accretion flow (diskir[23] in the Xspec notation). In this model, the X-ray emission consists of thermal radiation from the disk and a hard tail produced by comptonization of soft seed photons in a hot plasma of energetic electrons. A fraction of this radiation is intercepted by the outer regions of the disk, reprocessed and re-emitted in the optical and UV bands. This model often describes well the broadband emission of bright LMXB systems. The column density was again fixed to $N_{\mathrm{H}} = 2.1\times10^{21}$ cm^{-2} in the spectral fit. We obtained a statistically acceptable description of the data, with a reduced χ^2 of $\chi^2_{\mathrm{red}} = 0.89$ for 152 degrees of freedom. Results are listed in Supplementary Table 2. According to this model, the inner disk has an intrinsic (that is, not irradiated) temperature of ~200 eV and a radius of ~25 km (inferred from the model normalization and assuming an inclination angle of ~50°, as derived from modelling of the multi-band light curve in quiescence using a Markov chain Monte Carlo technique[18]). Seed photons from the inner disk are Comptonized by the hot-electron cloud close to the neutron star (or possibly within the accretion column) to produce the continuum observed in the X-ray band; the electron temperature of this component was fixed to the value found from modelling of the X-ray spectrum[47], while the photon index was allowed to vary (best-fitting value of $\Gamma = 2.76\pm0.06$). A fraction $7.1^{+1.5}_{-1.2}\%$ of this hard flux is reprocessed in the outer disk, whose radius is about 10^4 times larger than the inner disk radius, $R_{\mathrm{out}} \approx 10^{10}$ cm. This is comparable to the size of the Roche lobe of the neutron star and thus the size of the disk.

To investigate the origin of the pulsed emission in the optical/UV band, we also extracted the pulsed SED on 7–8 August 2019. For the X-ray band, we first evaluated the values for the background-subtracted pulse r.m.s. amplitudes over the energy ranges 0.5–1, 1–2 and 2–3 keV, as well as the 3σ upper limits over the ranges 3–5 and 5–10 keV. We calculated the de-absorbed X-ray fluxes over these same energy ranges by extrapolating the best-fitting model for the total emission (pulsed plus unpulsed), and multiplied them by the corresponding values (or upper limits) of the pulse r.m.s. amplitude to obtain integrated pulsed fluxes. We then multiplied the values so evaluated for the ratio between the mid-point energy of the interval and the width of the energy interval to derive pulsed fluxes (and upper limits) in νF_ν units, where ν is the frequency and F_ν is the flux per unit frequency. To convert the pulsed optical fluxes into νF_ν units, we multiplied dereddened fluxes by the filter full-width at half-maximum (89 nm, 84 nm, 158 nm and 154 nm for the B, V, R and i′ filters, respectively; we converted the AB magnitude of filter i′ to the Vega system). We then co-added the fluxes in the four different bands to obtain one single value for the pulsed flux covering the SiFAP2 operating band (320–900 nm) and multiplied this value by the optical pulse fractional amplitude. A total of four SED data points were obtained in this way (Supplementary Fig. 9), not enough to perform a meaningful modelling. We could test just two-parameter models on these data, such as blackbody, thermal emission from the disk, bremsstrahlung, and power law. A power-law model fit to the SED data points for the pulsed optical and X-ray emissions yields a reduced χ^2 value of $\chi^2_{\rm red} = 0.4$ for 2 degrees of freedom, and a functional dependence of the form $\nu F_\nu \propto \nu^{(0.62\pm0.04)}$.

Models. The fundamental photon cyclotron energy emitted by electrons in the magnetic field of SAX J1808.4−3658 at the base of the accretion column ($B \approx 3.5\times10^8$ G; refs. [24,66,67]) is $E_{\rm cyc} = 11.6(B\,/\,10^{12}\,{\rm G})\,{\rm keV} \approx 4.1(r\,/\,R_{\rm NS})^{-3}\,{\rm eV}$. At these energies, the UV and optical pulsed luminosity produced by optically thick cyclotron emission can be estimated as[25] $L_{\rm cyc} = A\int_{\nu_1}^{\nu_2}(2\pi kT_{\rm e}\nu^2/3c^2){\rm d}\nu$, where ν_1 and ν_2 are the boundary frequencies in the SiFAP2 or STIS/G230L energy range and $kT_{\rm e}$ is the electron temperature. $A \approx \pi R_{\rm NS}^2(R_{\rm NS}/r_{\rm c})$ is the hotspot area of the accreting polar cap[68], where $R_{\rm NS} = 10$ km is the neutron star radius and $r_{\rm c}$ is the corotation radius (the distance at which the Keplerian velocity of matter in the disk equals the velocity of the neutron star magnetosphere). The area of the accreting region is ~100 km^2 at most. The maximum cyclotron luminosity (using[69] $kT_{\rm e} = 100$ keV) from electrons in the accretion column is $L_{\rm cyc(opt)} \approx 10^{29}\,{\rm erg\,s^{-1}}$ in the 320–900 nm band and $L_{\rm cyc(UV)} \approx 6\times10^{29}\,{\rm erg\,s^{-1}}$ in the 165–310 nm band. These values are orders of magnitude smaller than the observed UV and optical pulsed luminosity, and do not favour a cyclotron emission scenario for the UV and optical bands.

An alternative scenario involves the presence of the accretion disk that does not prevent the rotation-powered mechanism from working. In this way, optical and UV pulsations could be produced by a rotation-driven pulsar, as in the isolated neutron stars[5,70,71]. The long-term spin-down energy loss rate can be estimated as $\dot{E}_{\rm sd} = 4\pi^2 I\nu\dot{\nu} \approx 2\times10^{34}\,{\rm erg\,s^{-1}}$, where I is the moment of inertia of the neutron star, ν is the neutron star spin frequency (Table 1) and $\dot{\nu}$ is the first time derivative of the neutron star spin frequency[4]. Comparing this value with the observed pulsed luminosity leads to the magneto-rotational efficiencies for SAX J1808.4−3658 of $\eta_{\rm UV} \approx 1\times10^{-2}$ and $\eta_{\rm opt} \approx 6\times10^{-4}$ in the B band with $\eta_{\rm UV/opt} = L_{\rm pulsed(UV/opt)}/\dot{E}_{\rm sd}$ computed at the time of our observations. Optical and UV pulses have been observed only in five rotation-powered pulsars[29,72], all isolated, slower-rotating, younger and with high magnetic fields ($>10^{12}$ G). The efficiency in converting spin-down power to UV/optical luminosity was determined in PSR B0540−69 and in the Crab pulsar[14,29]. Our estimates are orders of magnitude higher than the Crab pulsar efficiencies of $\eta_{\rm UV} \approx 2\times10^{-5}$ in the 165–310 nm band and $\eta_{\rm opt} \approx 5\times10^{-6}$ in the B band. These high efficiencies in SAX J1808.4−3658 would call for the existence of a (so far unknown) physical process that is able to enhance the spin-down powered emission in the presence of an accretion disk.

Comparison between SAX J1808.4–3658 and PSR J1023+0038. Before SAX J1808.4−3658, fast optical pulsations were detected only from the transitional millisecond pulsar PSR J1023+0038 (ref. [14]) while it was lingering in an X-ray sub-luminous disk state at an average (0.5–10 keV) X-ray luminosity of $L_{\rm X} \approx 4\times10^{33}\,{\rm erg\,s^{-1}}$. The pulsed optical luminosity was also high in that case ($\approx10^{31}\,{\rm erg\,s^{-1}}$), considering that the source was releasing a spin-down power of $4.3\times10^{34}\,{\rm erg\,s^{-1}}$ in the radio pulsar state. Optical and X-ray pulses were almost phase aligned and detected only during the so-called ‘high’ X-ray luminosity mode in which the source spends ~70% of the time, but were seen to suddenly disappear in the lower luminosity mode, suggesting a common underlying process[15]. Both the optical and X-ray pulsations observed from PSR J1023+0038 are thought to originate from synchrotron radiation in the intrabinary shock just beyond the light cylinder radius, where the wind of relativistic particles ejected by the pulsar meets the accretion disk[15–17]. Optical pulsations from SAX J1808.4−3658 were detected in an intermediate stage of the outburst, when the X-ray luminosity had not yet peaked. Yet, the corresponding X-ray luminosity exceeded that of PSR J1023+0038 by about an order of magnitude ($L_{\rm X} \approx 6\times10^{34}\,{\rm erg\,s^{-1}}$). Optical pulses lagged the X-ray ones by ~1.4 ms, that is, they were almost in anti-phase. During this outburst and the previous ones, the X-ray spectral and timing properties of SAX J1808.4−3658 did not show any evidence for transitions to a non-accreting regime. These arguments suggest that its X-ray, UV and optical pulses can hardly be explained by invoking the same physical mechanism.

Data availability

Source data are provided with this paper. The barycentered SiFAP2 data that support the findings of this study are available in figshare at https://doi.org/10.6084/m9.figshare.12707444.

Received: 2 October 2019; Accepted: 14 January 2021;
Published online: 22 February 2021

References

1. Alpar, M. A., Cheng, A. F., Ruderman, M. A. & Shaham, J. A new class of radio pulsars. *Nature* **300**, 728–730 (1982).
2. Wijnands, R. & van der Klis, M. A millisecond pulsar in an X-ray binary system. *Nature* **394**, 344–346 (1998).
3. Campana, S. & Di Salvo, T. Accreting pulsars: mixing-up accretion phases in transitional systems. *Astrophys. Space Sci. Library* **457**, 149–184 (2018).
4. Bult, P. et al. Timing the pulsations of the accreting millisecond pulsar SAX J1808.4−3658 during its 2019 outburst. *Astrophys. J.* **898**, 38 (2020).
5. Torres, D. F. Order parameters for the high-energy spectra of pulsars. *Nat. Astron.* **2**, 247–256 (2018).
6. Harding, A. K., Kalapotharakos, C., Barnard, M. & Venter, C. Multi-TeV emission from the Vela pulsar. *Astrophys. J. Lett.* **869**, L18 (2018).
7. Chakrabarty, D. & Morgan, E. H. The two-hour orbit of a binary millisecond X-ray pulsar. *Nature* **394**, 346–348 (1998).
8. Archibald, A. M. et al. A radio pulsar/X-ray binary link. *Science* **324**, 1411–1414 (2009).
9. Papitto, A. et al. Swings between rotation and accretion power in a binary millisecond pulsar. *Nature* **501**, 517–520 (2013).
10. Watts, A. L. et al. Colloquium: measuring the neutron star equation of state using x-ray timing. *Rev. Mod. Phys.* **88**, 021001 (2016).
11. Wijnands, R. in *Trends in Pulsar Research* (ed. Lowry, J. A.) Ch. 3 (Nova Science, 2006).
12. Patruno, A. & Watts, A. L. in *Timing Neutron Stars: Pulsations, Oscillations and Explosions* (eds Belloni, T. et al.) 143–208 (Springer, 2021).
13. Liu, Q. Z., van Paradijs, J. & van den Heuvel, E. P. J. A catalogue of low-mass X-ray binaries in the Galaxy, LMC, and SMC (Fourth edition). *Astron. Astrophys.* **469**, 807–810 (2007).
14. Ambrosino, F. et al. Optical pulsations from a transitional millisecond pulsar. *Nat. Astron.* **1**, 854–858 (2017).
15. Papitto, A. et al. Pulsating in unison at optical and X-ray energies: simultaneous high time resolution observations of the transitional millisecond pulsar PSR J1023+0038. *Astrophys. J.* **882**, 104 (2019).
16. Veledina, A., Nättilä, J. & Beloborodov, A. M. Pulsar wind-heated accretion disk and the origin of modes in transitional millisecond pulsar PSR J1023+0038. *Astrophys. J.* **884**, 144 (2019).
17. Campana, S. et al. Probing X-ray emission in different modes of PSR J1023+0038 with a radio pulsar scenario. *Astron. Astrophys.* **629**, L8 (2019).
18. Wang, Z. et al. Multiband studies of the optical periodic modulation in the X-ray binary SAX J1808.4−3658 during its quiescence and 2008 outburst. *Astrophys. J.* **765**, 151 (2013).
19. Galloway, D. K. & Cumming, A. Helium-rich thermonuclear bursts and the distance to the accretion-powered millisecond pulsar SAX J1808.4−3658. *Astrophys. J.* **652**, 559–568 (2006).
20. Gilfanov, M. et al. The millisecond X-ray pulsar/burster SAX J1808.4−3658: the outburst light curve and the power law spectrum. *Astron. Astrophys.* **338**, L83–L86 (1998).
21. Stella, L., Campana, S., Mereghetti, S., Ricci, D. & Israel, G. L. The discovery of quiescent X-ray emission from SAX J1808.4−3658, the transient 2.5 millisecond pulsar. *Astrophys. J. Lett.* **537**, L115–L118 (2000).
22. Giles, A. B., Hill, K. M. & Greenhill, J. G. The optical counterpart of SAX J1808.4−3658, the transient bursting millisecond X-ray pulsar. *Mon. Not. R. Astron. Soc.* **304**, 47–51 (1999).
23. Gierliński, M., Done, C. & Barret, D. Phase-resolved X-ray spectroscopy of the millisecond pulsar SAX J1808.4−3658. *Mon. Not. R. Astron. Soc.* **331**, 141–153 (2002).
24. Burderi, L. et al. Order in the chaos: spin-up and spin-down during the 2002 outburst of SAX J1808.4−3658. *Astrophys. J. Lett.* **653**, L133–L136 (2006).
25. Thompson, A. M. & Cawthorne, T. V. Cyclotron emission from white dwarf accretion columns. *Mon. Not. R. Astron. Soc.* **224**, 425–434 (1987).
26. Basko, M. M. & Sunyaev, R. A. Radiative transfer in a strong magnetic field and accreting X-ray pulsars. *Astron. Astrophys.* **42**, 311–321 (1975).
27. Melrose, D. B. Coherent emission mechanisms in astrophysical plasmas. *Rev. Mod. Plasma Phys.* **1**, 5 (2017).
28. Pacini, F. & Salvati, M. The optical luminosity of very fast pulsars. *Astrophys. J.* **274**, 369–371 (1983).
29. Mignani, R. P. Optical, ultraviolet, and infrared observations of isolated neutron stars. *Adv. Space Res.* **47**, 1281–1293 (2011).
30. Parfrey, K. & Tchekhovskoy, A. General-relativistic simulations of four states of accretion onto millisecond pulsars. *Astrophys. J. Lett.* **851**, L34 (2017).
31. Parfrey, K., Spitkovsky, A. & Beloborodov, A. M. Torque enhancement, spin equilibrium, and jet power from disk-induced opening of pulsar magnetic fields. *Astrophys. J.* **822**, 33 (2016).
32. Kluźniak, W. & Rappaport, S. Magnetically torqued thin accretion disks. *Astrophys. J.* **671**, 1990–2005 (2007).
33. Coroniti, F. V. Magnetically striped relativistic magnetohydrodynamic winds: the Crab Nebula revisited. *Astrophys. J.* **349**, 538 (1990).
34. Kirk, J. G., Skjæraasen, O. & Gallant, Y. A. Pulsed radiation from neutron star winds. *Astron. Astrophys. Lett.* **388**, L29–L32 (2002).

35. Rybicki, G. B. & Lightman, A. P. *Radiative Processes In Astrophysics* (Wiley, 1979).
36. Ghedina, A. et al. SiFAP2: a new versatile configuration at the TNG for the MPPC based photometer. *Proc. SPIE* **10702**, 107025Q (2018).
37. Meddi, F. et al. A new fast silicon photomultiplier photometer. *Publ. Astron. Soc. Pac.* **124**, 448–453 (2012).
38. Ambrosino, F. et al. The latest version of SiFAP: beyond microsecond time scale photometry of variable objects. *J. Astron. Instrum.* **5**, 1650005 (2016).
39. Hartman, J. M. et al. The long-term evolution of the spin, pulse shape, and orbit of the accretion-powered millisecond pulsar SAX J1808.4−3658. *Astrophys. J.* **675**, 1468–1486 (2008).
40. Gendreau, K. C. et al. The Neutron star Interior Composition Explorer (NICER): design and development. *Proc. SPIE* **9905**, 99051H (2016).
41. Gendreau, K. & Arzoumanian, Z. Searching for a pulse. *Nat. Astron.* **1**, 895 (2017).
42. Papitto, A. et al. Spin down during quiescence of the fastest known accretion-powered pulsar. *Astron. Astrophys.* **528**, A55 (2011).
43. Leahy, D. A., Elsner, R. F. & Weisskopf, M. C. On searches for periodic pulsed emission—the Rayleigh test compared to epoch folding. *Astrophys. J.* **272**, 256–258 (1983).
44. Leahy, D. A. Searches for pulsed emission—improved determination of period and amplitude from epoch folding for sinusoidal signals. *Astron. Astrophys.* **180**, 275–277 (1987).
45. Buccheri, R. et al. Search for pulsed γ-ray emission from radio pulsars in the COS-B data. *Astron. Astrophys.* **128**, 245–251 (1983).
46. Foight, D. R., Güver, T., Özel, F. & Slane, P. O. Probing X-ray absorption and optical extinction in the interstellar medium using Chandra observations of supernova remnants. *Astrophys. J.* **826**, 66 (2016).
47. Di Salvo, T. et al. NuSTAR and XMM-Newton broad-band spectrum of SAX J1808.4-3658 during its latest outburst in 2015. *Mon. Not. R. Astron. Soc.* **483**, 767–779 (2019).
48. Fitzpatrick, E. L. Correcting for the effects of interstellar extinction. *Publ. Astron. Soc. Pac.* **111**, 63–75 (1999).
49. Schlafly, E. F. & Finkbeiner, D. P. Measuring reddening with Sloan Digital Sky Survey stellar spectra and recalibrating SFD. *Astrophys. J.* **737**, 103 (2011).
50. Elebert, P. et al. Optical spectroscopy and photometry of SAX J1808.4−3658 in outburst. *Mon. Not. R. Astron. Soc.* **395**, 884–894 (2009).
51. Tudor, V. et al. Disc-jet coupling in low-luminosity accreting neutron stars. *Mon. Not. R. Astron. Soc.* **470**, 324–339 (2017).
52. Russell, D. M. et al. Optical precursors to X-ray binary outbursts. *Astron. Nach.* **340**, 278–283 (2019).
53. Pirbhoy, S. F. et al. XB-NEWS detection of a new outburst of MAXI J1348−630. *The Astronomer's Telegram* 13451 (2020).
54. Roming, P. W. A. et al. The Swift Ultra-Violet/Optical Telescope. *Space Sci. Rev.* **120**, 95–142 (2005).
55. Gehrels, N. et al. The Swift Gamma-Ray Burst Mission. *Astrophys. J.* **611**, 1005–1020 (2004).
56. Arnaud, K. A. in *Astronomical Data Analysis Software and Systems* (eds Jacoby, G. H. & Barnes, J.) 17–20 (Astronomical Society of the Pacific, 1996).
57. Życki, P. T., Done, C. & Smith, D. A. The 1989 May outburst of the soft X-ray transient GS 2023+338 (V404 Cyg). *Mon. Not. R. Astron. Soc.* **309**, 561–575 (1999).
58. Verner, D. A., Ferland, G. J., Korista, K. T. & Yakovlev, D. G. Atomic data for astrophysics. II. New analytic FITS for photoionization cross sections of atoms and ions. *Astrophys. J.* **465**, 487 (1996).
59. Wilms, J., Allen, A. & McCray, R. On the absorption of X-rays in the interstellar medium. *Astrophys. J.* **542**, 914–924 (2000).
60. Papitto, A. et al. XMM-Newton detects a relativistically broadened iron line in the spectrum of the ms X-ray pulsar SAX J1808.4−3658. *Astron. Astrophys.* **493**, L39–L43 (2009).
61. Sanna, A. et al. NuSTAR observation of the latest outburst of SAX J1808.4−3658. *The Astronomer's Telegram* 13022 (2019).
62. in 't Zand, J. J. M. et al. Discovery of the X-ray transient SAX J1808.4−3658, a likely low-mass X-ray binary. *Astron. Astrophys. Lett.* **331**, L25–L28 (1998).
63. Vrtilek, S. D. et al. Observations of Cygnus X-2 with IUE: ultraviolet results from a multiwavelength campaign. *Astron. Astrophys.* **235**, 162 (1990).
64. van Paradijs, J. & McClintock, J. E. in *X-ray Binaries* (eds Lewin, W. H. G. et al.) 58–125 (Cambridge Univ. Press, 1995).
65. Russell, D. M. et al. Global optical/infrared-X-ray correlations in X-ray binaries: quantifying disc and jet contributions. *Mon. Not. R. Astron. Soc.* **371**, 1334–1350 (2006).
66. Di Salvo, T. & Burderi, L. Constraints on the neutron star magnetic field of the two X-ray transients SAX J1808.4−3658 and Aql X−1. *Astron. Astrophys.* **397**, 723–727 (2003).
67. Sanna, A. et al. On the timing properties of SAX J1808.4−3658 during its 2015 outburst. *Mon. Not. R. Astron. Soc.* **471**, 463–477 (2017).
68. Frank, J., King, A. & Raine, D. J. (eds) *Accretion Power in Astrophysics* (Cambridge Univ. Press, 2002).
69. Poutanen, J. & Gierliński, M. On the nature of the X-ray emission from the accreting millisecond pulsar SAX J1808.4−3658. *Mon. Not. R. Astron. Soc.* **343**, 1301–1311 (2003).
70. Romani, R. W. Gamma-ray pulsars: radiation processes in the outer magnetosphere. *Astrophys. J.* **470**, 469 (1996).
71. Torres, D. F., Viganò, D., Coti Zelati, F. & Li, J. Synchrocurvature modelling of the multifrequency non-thermal emission of pulsars. *Mon. Not. R. Astron. Soc.* **489**, 5494–5512 (2019).
72. Mignani, R. P. et al. The first ultraviolet detection of the Large Magellanic Cloud pulsar PSR B0540−69 and its multi-wavelength properties. *Astrophys. J.* **871**, 246 (2019).

Acknowledgements

A.M.Z. thanks the HST contact scientist, D. Welty (STScI), for constant support in the observation planning and T. Royle (STScI) for checking the scheduling processes. A.M.Z. thanks A. Riley (STIS Team) for the support in the scientific data analysis. A.M.Z. acknowledges the support of the PHAROS COST Action (CA16214) and A. Ridolfi for his help in data analysis. A.M.Z. would also like to thank G. Benevento for comments on draft. F.C.Z. is supported by a Juan de la Cierva fellowship. S.C. and P.D.A. acknowledge support from ASI grant I/004/11/3. D.d.M., A.P. and L.S. acknowledge financial support from the Italian Space Agency (ASI) and National Institute for Astrophysics (INAF) under agreements ASI-INAF I/037/12/0. L.B., D.d.M., T.D.S., A.P. and L.S. acknowledge financial contributions from ASI-INAF agreement no. 2017-14-H.0, INAF main-stream (principal investigator: T. Belloni; principal investigator: A. De Rosa). D.F.T. acknowledges support from grants PGC2018-095512-B-I00, SGR2017-1383 and AYA2017-92402-EXP. L.B and T.D.S. thank A. Marino for useful discussions and acknowledge financial contributions from the HERMES project financed by the Italian Space Agency (ASI) agreement no. 2016/13 U.O. T.D.S. and L.S. acknowledge the iPeska research grant (principal investigator: A. Possenti) funded under the INAF national call Prin-SKA/CTA approved with the Presidential Decree 70/2016. A.P., F.C.Z., and D.T. acknowledge the International Space Science Institute (ISSI-Beijing), which funded and hosted the international team 'Understanding and Unifying the Gamma-rays Emitting Scenarios in High Mass and Low Mass X-ray Binaries'. Results obtained with SiFAP2 and presented in this paper are based on observations made with the Italian Telescopio Nazionale Galileo (TNG) operated by the Fundación Galileo Galilei (FGG) of the Istituto Nazionale di Astrofisica (INAF) at the Observatorio del Roque de los Muchachos (La Palma, Canary Islands, Spain). Part of this paper is based on observations with the NASA/ESA Hubble Space Telescope, obtained at the Space Telescope Science Institute, which is operated by AURA, Inc., under NASA contract NAS5-26555. This work also made use of data and software provided by the High Energy Astrophysics Science Archive Research Center (HEASARC).

Author contributions

F.A., A.M.Z., A.P. and F.C.Z. analysed optical, UV and X-ray data. F.A., A.M.Z., A.P., F.C.Z. and L.S. wrote the paper. A.M.Z., A.P., S.C., P.D.A., F.C.Z., P.C., L.S., T.D.S., L.B., D.d.M., D.F.T., G.L.I. and A.S. interpreted the results. F.A., F.M., P. Cretaro, A.G., F. Leone. and E.P. conceived SiFAP2. A.G., A.P. and F.A. performed the optical observation. A.G., M. Cecconi, M.D.G.G., A.L.R.R., H.P.V., M.H.D. and J.J.S.J. developed the SiFAP2 mechanical interface and its relative control software. M. Cadelano and R.P.M. contributed to the HST data analysis. M.C.B., D.M.R., D.M.B. and F. Lewis. contributed to the optical part of the SED. All authors read, commented on and approved the submission of this article.

Competing interests

The authors declare no competing interests.

Additional information

Supplementary information The online version contains supplementary material available at https://doi.org/10.1038/s41550-021-01308-0.

Correspondence and requests for materials should be addressed to F.A. or A.M.Z.

Peer review information *Nature Astronomy* thanks Lucien Kuiper and Jumpei Takata for their contribution to the peer review of this work.

Reprints and permissions information is available at www.nature.com/reprints.

Publisher's note Springer Nature remains neutral with regard to jurisdictional claims in published maps and institutional affiliations.